CHEMISTRY OF MATERIALS

pubs.acs.org/cm

Article

Exploiting the Transformative Features of Metal Halides for the Synthesis of $CsPbBr_3$@SiO_2 Core–Shell Nanocrystals

Christian Rossi, Riccardo Scarfiello, Rosaria Brescia, Luca Goldoni, Gianvito Caputo, Luigi Carbone, Diego Colombara,* Luca De Trizio, Liberato Manna, and Dmitry Baranov*

Cite This: *Chem. Mater.* 2022, 34, 405–413

Read Online

ACCESS | Metrics & More | Article Recommendations | Supporting Information

ABSTRACT: The encapsulation of colloidal lead halide perovskite nanocrystals within silica (SiO_2) is one of the strategies to protect them from polar solvents and other external factors. Here, we demonstrate the overcoating of $CsPbBr_3$ perovskite nanocrystals with silica by exploiting the anhydride-induced transformation of Cs_4PbBr_6 nanocrystals. $CsPbBr_3$@SiO_2 core–shell nanocrystals are obtained after (i) a reaction between colloidal Cs_4PbBr_6 nanocrystals and maleic anhydride in toluene that yields $CsPbBr_3$ nanocrystals and maleamic acid and (ii) a silica-shell growth around $CsPbBr_3$ nanocrystals via hydrolysis of added alkoxysilanes. The reaction between Cs_4PbBr_6 nanocrystals and maleic anhydride is necessary to promote shell formation from alkoxysilanes, as demonstrated in control experiments. The best samples of as-prepared $CsPbBr_3$@SiO_2 nanocrystals consist of ∼10 nm single-crystal $CsPbBr_3$ cores surrounded by ∼5–7 nm amorphous silica shell. Despite their core–shell structure, such nanostructures are poor emitters and degrade within minutes of exposure to ethanol. The photoluminescence intensity of the core–shell nanocrystals is improved by the treatment with a solution of $PbBr_2$ and ligands, and their stability in ethanol is extended to several days after applying an additional silica growth step. Overall, the investigated approach outlines a strategy for making colloidal core–shell nanocrystals utilizing the transformative chemistry of metal halides and reveals interesting insights regarding the conditions required for $CsPbBr_3$@SiO_2 nanocrystal formation.

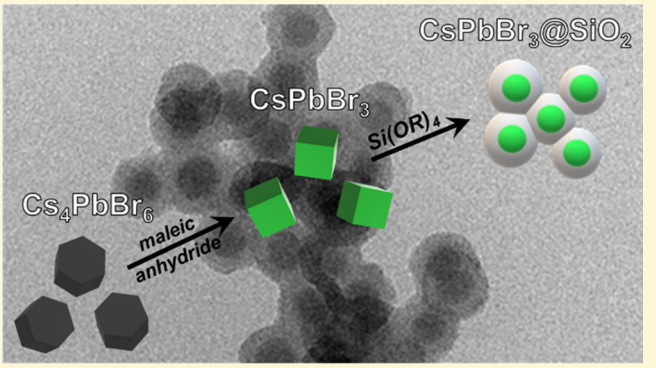

INTRODUCTION

Lead halide perovskites (LHPs) are emerging semiconductor materials that promise to revolutionize optoelectronic devices such as photodetectors, solar concentrators, scintillators, solar cells, and light-emitting diodes (LEDs).[1−7] Colloidal nanocrystals (NCs) of LHPs capped with long-chain organic ligands attracted the attention of many research groups due to their straightforward synthesis, strong light absorption, and bright and tunable photoluminescence (PL).[8−11] Despite their outstanding optoelectronic properties, LHP NCs suffer from several issues that constitute a hurdle for practical applications.

In particular, LHP NCs degrade and lose their bright PL upon excessive exposure to light and heat, and they do not tolerate polar solvents and acidic or alkaline environments.[12−14] To circumvent these issues, several strategies have been developed to improve stability, including the encapsulation of LHP NCs in inorganic oxides (e.g., SiO_2, Al_2O_3, TiO_2, etc.),[14−23] polymers,[24−28] metal halides,[29] and metal–organic frameworks (MOFs).[30−32] Encapsulating $CsPbBr_3$ NCs, a prototypical example of LHPs, in a polymer can stabilize them against water/humidity but does not always provide high thermal resistance.[33,24,27] MOFs and metal halide matrices provide good thermal stability, but it is often insufficient to protect the NCs against water.[30,34] In this regard, inorganic oxides are attractive encapsulants because they can provide both water and thermal stability to the NCs.[13,22,23,35]

Among the inorganic oxides, silica is a promising candidate, as it is transparent in the visible range, mechanically robust, and chemically inert. LHP NCs have been encapsulated in silica by two methods: by embedment in bulk silica or by growing LHP NCs inside the pores of mesoporous silica.[13,14,20−23] The heat-induced sealing of LHP NCs inside the mesoporous silica has delivered brightly photoluminescent composites with especially impressive stability against water and acidic media (e.g., 1 M aqueous HCl or aqua regia).[13,22] The fine tunability of green emission in the narrow 525–535 nm range has been demonstrated for such composites by mixing variable amounts of sodium into $CsPbBr_3$ NCs.[23] The

Received: October 29, 2021
Revised: December 15, 2021
Published: December 30, 2021

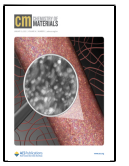

bulky composites are not optimal for technologies where a colloidal formulation is desired, for example in inkjet-printed LEDs and displays. Hence, obtaining luminescent LHP@SiO_2 core−shell NCs as colloidal dispersions would be advantageous due to the tunability of emitter content (for control over concentration quenching) and minimized scattering (due to the subwavelength grain size of the core−shell NCs). These reasons motivated our interest in pursuing the LHP@SiO_2 core−shell architecture.

Several groups have reported the fabrication of colloidally stable $CsPbBr_3$@SiO_2 core−shell NCs with thin shells and high photoluminescence quantum yield (PLQY).[36−42] The thin SiO_2 shells provide limited stability against polar solvents,[9,39] and growing thick shells has proven to be difficult. The complexity of growing thicker SiO_2 shells onto preformed $CsPbBr_3$ NCs arises from the fast degradation of the NCs during the coating process. The growth of silica is generally catalyzed by acids (e.g., HNO_3)[43] or bases (e.g., ammonia),[44] which can easily dissolve LHP NCs.[14] One strategy to circumvent this bottleneck is to utilize reactive metal halide NCs, such as Cs_4PbX_6 (X = Cl, Br, I), that transform into emissive LHP NCs under reaction conditions that are otherwise destructive to LHPs.[14] For example, Park et al. treated Cs_4PbBr_6 NCs with HNO_3 and tetraethyl orthosilicate (TEOS): the starting Cs_4PbBr_6 NCs were converted into $CsPbBr_3$ NCs under acidic conditions, and the simultaneous TEOS hydrolysis led to the formation of a silica matrix around them.[14] Such a procedure provided a route for the scalable synthesis of bulk LHP/SiO_2 composites but was unable to deliver well-defined $CsPbBr_3$@SiO_2 NCs due to the fast course of the reactions.

We hypothesize that under milder reaction conditions compared to those of Park et al.,[14] it is possible to convert Cs_4PbBr_6 NCs into $CsPbBr_3$ NCs and coat the resulting NCs with a SiO_2 shell. To do so, we took inspiration from the reactivity between poly(maleic anhydride-alt-1-octadecene) and Cs_4PbBr_6 NCs that yields emissive perovskite $CsPbBr_3$ NCs.[45] The conversion entails the reaction of the maleic anhydride (MANH) functional group of the polymer with oleylamine (OLAM), which is present both as a free molecule in the colloidal suspension and as a capping ligand on the surface of Cs_4PbBr_6 NCs, and results in the formation of maleamic acid.[45−47]

In this work, instead of the polymer, we used its reactive fragment—the small MANH molecule—to trigger the Cs_4PbBr_6 → $CsPbBr_3$ NCs transformation and to acidify the reaction medium, thus catalyzing silica growth (Scheme 1, steps 1 and 2). The MANH-assisted conversion of Cs_4PbBr_6 NCs generated $CsPbBr_3$ NCs bearing a surface that was suitable to both promote and withstand a silica shell growth. As-synthesized $CsPbBr_3$@SiO_2 core−shell NCs demonstrated low PLQY (1−4%) and lost their PL after ∼15 min of exposure to ethanol. An additional treatment of core−shell NCs with $PbBr_2$, dissolved in the mixture of oleic acid (OA) and OLAM, (Scheme 1, step 3) increased PLQY up to 8%, and additional growth of silica (Scheme 1, step 4) significantly extended their stability in ethanol (a negligible loss of PL intensity after ∼9 days). Overall, the developed synthetic procedure expands the reaction toolbox available to chemists exploring the reactivity of metal halide NCs.

Scheme 1. Principal Steps in the Synthesis of $CsPbBr_3$@SiO_2 Core−Shell NCs[a]

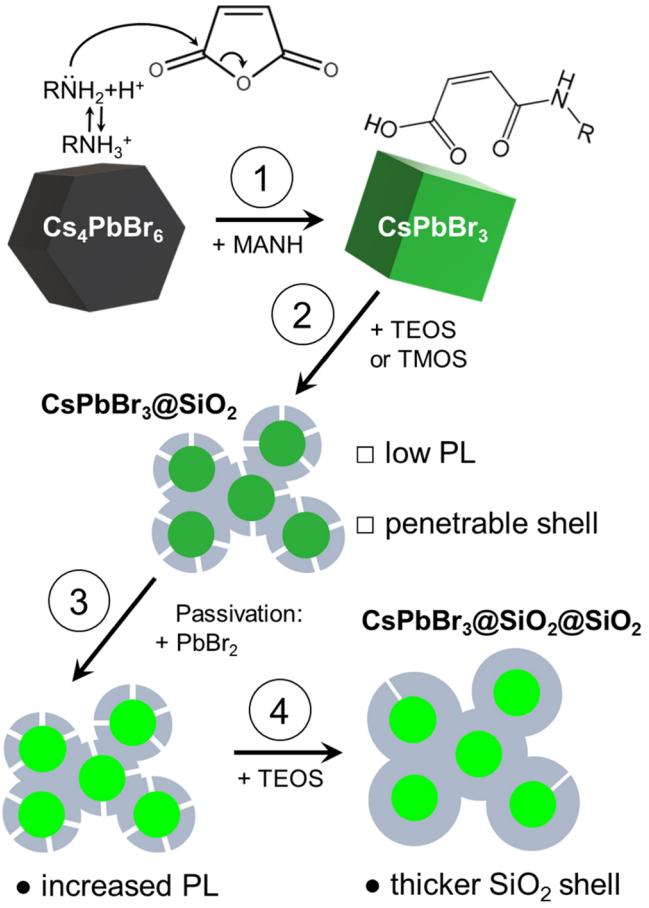

[a]The process starts from Cs_4PbBr_6 NCs that are converted to $CsPbBr_3$@SiO_2 NCs via reactions with maleic anhydride (MANH, step 1) and alkoxysilanes (TEOS or TMOS, tetraethyl or tetramethyl orthosilicate, respectively, step 2). The optical properties of the core−shell NCs are enhanced by treating them with $PbBr_2$ dissolved in the mixture of ligands (step 3) and by overgrowth of a thicker silica shell (step 4).

EXPERIMENTAL SECTION

Materials. Cesium carbonate (Cs_2CO_3, 99%), lead bromide ($PbBr_2$, ≥98%), OA (90%), OLAM (70%), 1-octadecene (ODE, 90%), ethyl acetate (≥99.5%), toluene (≥99.7%), anhydrous toluene (99.8%), deuterated toluene, MANH (99%), TEOS (>99.5% and the 99.999% for the air-free experiment), and tetramethyl orthosilicate (TMOS, ≥99%) were purchased from Sigma Aldrich and used as received, except for OA and OLAM, which were degassed prior to use in the air-free experiment. Milli-Q water was obtained from the Millipore purification station installed in the laboratory. A MANH stock solution (0.34 M) was prepared by dissolving 500 mg of MANH in 15 mL of toluene. The OLAM-iodide (OLAM-I) complex for halide exchange reactions was prepared according to the procedure detailed in ref 48. With the exception of Cs_4PbBr_6 NC synthesis, and unless stated otherwise, all the reactions were run under air at room temperature (∼21 °C). The reaction time started when the MANH solution was added.

Cs_4PbBr_6 NC Synthesis. The Cs_4PbBr_6 NCs were prepared via the hot-injection method of Akkerman et al. with a few modifications.[49] Specifically, a Cs-oleate precursor solution was prepared by dissolving 400 mg of Cs_2CO_3 in 8 mL of OA at 100 °C in a 20 mL vial under stirring and N_2 flow. A $PbBr_2$−precursor solution was prepared in a preweighed 20 mL vial by mixing 72 mg

https://doi.org/10.1021/acs.chemmater.1c03749
Chem. Mater. 2022, 34, 405−413

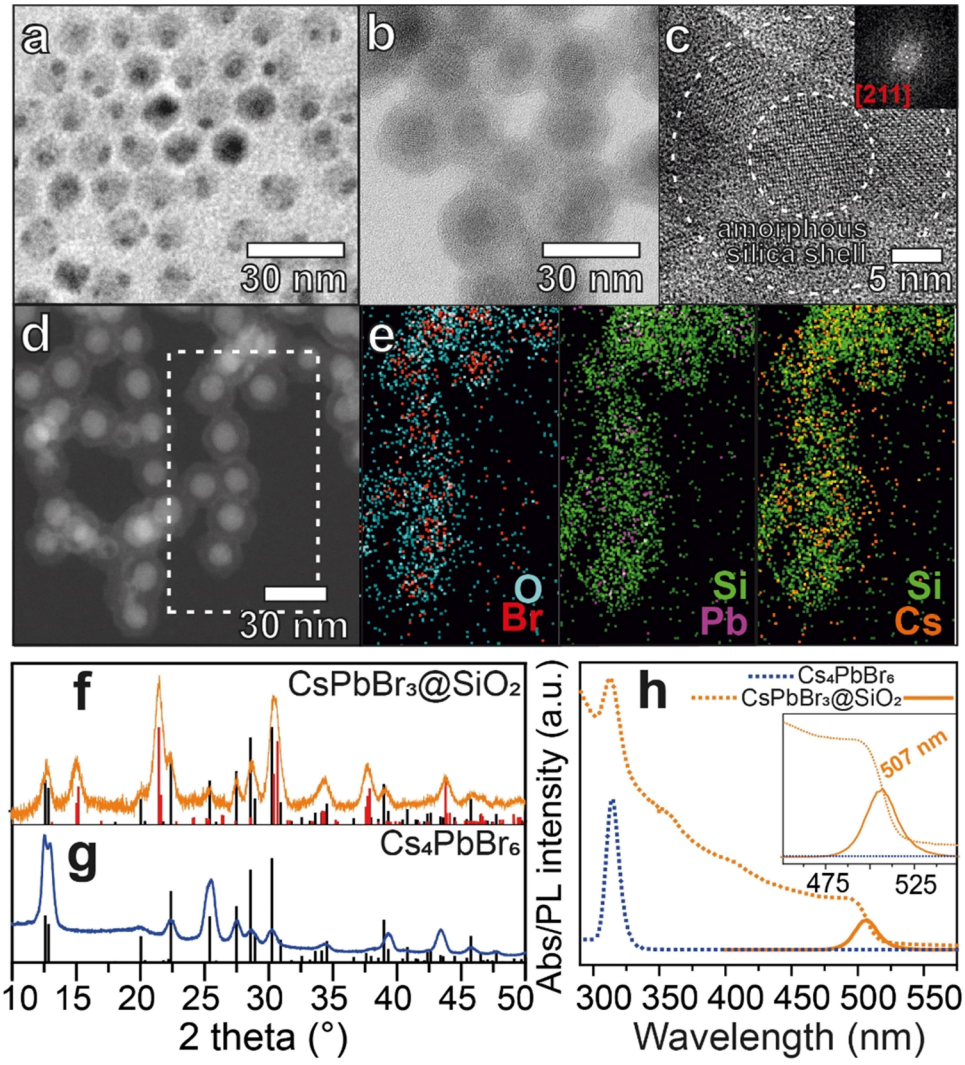

Figure 1. Characterization of the best sample of $CsPbBr_3@SiO_2$ NCs prepared via the one-step procedure. (a) BF-TEM image of starting Cs_4PbBr_6 NCs; dark spots are Pb^0 domains likely formed under the electron beam;[52] (b) BF-TEM image of $CsPbBr_3@SiO_2$ NCs; (c) HR-TEM image of a $CsPbBr_3@SiO_2$ NC; the inset shows a fast Fourier transform of the $CsPbBr_3$ core, matching better with the cubic $CsPbBr_3$ phase (ICSD code 97852) than with the orthorhombic phase, likely due to polymorphism in $CsPbBr_3$ NCs;[53] (d) HAADF-STEM image of $CsPbBr_3@SiO_2$ NCs and (e) corresponding color maps of the distribution of elements obtained with EDS from the sample area indicated by a white dashed box; (f, g) XRD patterns of $CsPbBr_3@SiO_2$ NCs and starting Cs_4PbBr_6 NCs, respectively. The experimental XRD patterns are compared with reference powder diffraction data for rhombohedral Cs_4PbBr_6 (black bars, ICSD code 162158) and orthorhombic $CsPbBr_3$ (red bars, COD code 4510745); (h) PL and absorption spectra of starting Cs_4PbBr_6 NCs and $CsPbBr_3@SiO_2$ NCs.

(0.2 mmol) of $PbBr_2$, 5 mL (15.6 mmol) of ODE, 1.5 mL (4.5 mmol) of OLAM, and 0.2 mL (0.63 mmol) of OA. The vial was placed under stirring into a machined aluminum block preheated to about 150 °C on top of a hot plate. The $PbBr_2$−precursor mixture was left under stirring for about 15 min at ∼100−120 °C. During this time, the vacuum was applied for a few minutes until the solution stopped bubbling, and at that point, the vacuum was replaced with nitrogen flux. Once all $PbBr_2$ was dissolved by visual inspection, the vial was transferred into a secondary hot plate, and the temperature of the reaction mixture was let to stabilize at 80 °C. At that point, 0.8 mL of the Cs-oleate precursor was swiftly injected inside the $PbBr_2$−precursor at 80 °C through a 1 mL syringe equipped with a 16G needle. An initially clear reaction mixture acquired a cloudy-white appearance over the course of ∼30 s. After an additional 30 s, the vial was moved into a water-ice bath to quench the reaction. To isolate the Cs_4PbBr_6 NCs, the cloudy-white mixture was centrifuged at 4000 rpm for 10 min, the supernatant was discarded, and the inner walls of the vials were thoroughly dried from the remaining liquid with a piece of paper tissue. After this, the vial with an NC solid was weighed again, and the NC solid was redispersed in the amount of nonanhydrous toluene needed to obtain 30 mg/mL dispersion of NCs. This dispersion is referred to as Cs_4PbBr_6 NC stock solution.

NC Transformations. Unless otherwise stated, all procedures below were carried out under air, at room temperature, using regular toluene as a solvent. The reported amounts of reagents and reaction times are for the optimized syntheses and might be adjusted on a batch-to-batch basis. To isolate the products of reactions, 500 μL of ethyl acetate was added to the sample followed by centrifugation at 4000 rpm for 10 min. The supernatant was discarded, and the inner walls of the vial were thoroughly dried from the remaining liquid with a piece of paper tissue, and the solid was redispersed in 500 μL of toluene for further characterization and experimentation.

$CsPbBr_3@SiO_2$ NC One-Step Synthesis. First, 100 μL of Cs_4PbBr_6 NC stock solution, 100 μL of toluene, 20 μL of OLAM, 30 μL of alkoxysilane (TEOS or TMOS), 1 mL of MANH stock solution, and, after a brief period of time (9 min for TMOS; 3 min for TEOS), 500 μL of OA were combined in this order in a 4 mL vial, which is kept under stirring (∼500 rpm) on a stir plate. The mixture was left to react for several hours (16 h for TMOS and 3 h for TEOS, unless mentioned otherwise) followed by isolation of the product.

https://doi.org/10.1021/acs.chemmater.1c03749
Chem. Mater. 2022, 34, 405−413

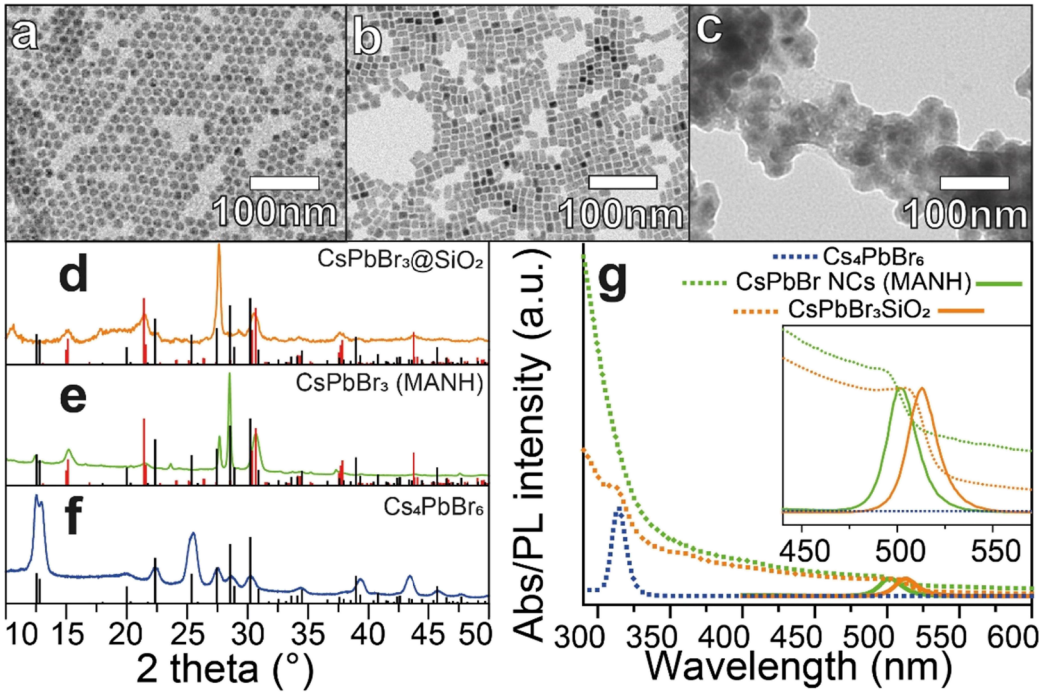

Figure 2. Characterization of the starting Cs_4PbBr_6 NCs, the $CsPbBr_3$ NCs isolated after the reaction with MANH, and the $CsPbBr_3$@SiO_2 NCs prepared via a two-step procedure. (a–c) BF-TEM images of Cs_4PbBr_6, $CsPbBr_3$, and $CsPbBr_3$@SiO_2 NCs, respectively. (d–f) XRD patterns of $CsPbBr_3$@SiO_2, $CsPbBr_3$, and Cs_4PbBr_6 NCs, respectively, along with the reference powder diffraction data (rhombohedral Cs_4PbBr_6 – black bars, ICSD code 162158; orthorhombic $CsPbBr_3$ – red bars, COD code 4510745). (g) Optical absorption and PL spectra of starting Cs_4PbBr_6, as-prepared $CsPbBr_3$, and $CsPbBr_3$@SiO_2 NCs.

$CsPbBr_3$@SiO_2 NC Two-Step Synthesis. First, 100 μL of Cs_4PbBr_6 NC stock solution, 100 μL of toluene, 20 μL of OLAM, and 1 mL of MANH stock solution were combined in this order in a 4 mL vial and kept under stirring (~500 rpm) on a stir plate. After 15 min of reaction, 100 μL of TEOS and 500 μL of OA were added in this order. The mixture was left to react for about 16 h followed by isolation of the product.

Cs_4PbBr_6 to $CsPbBr_3$ NC Conversion. First, 100 μL of Cs_4PbBr_6 NC stock solution, 100 μL of toluene, 20 μL of OLAM, and 1 mL of MANH stock solution were combined in this order in a 4 mL vial and kept under stirring (~500 rpm) on a stir plate for 15 min, after which the NCs were isolated.

Further Treatments of $CsPbBr_3$@SiO_2 NCs: Surface Passivation with $PbBr_2$ and the Thickening of the Silica Shell. A sample of $CsPbBr_3$@SiO_2 NCs prepared following the one-step procedure and the crude reaction mixture was split equally into two 4 mL vials and centrifuged at 4000 rpm for 10 min. The supernatant was discarded, and the precipitate was redispersed in 250 μL of toluene. Each sample was stirred at 500 rpm for the entire process. Then, 37.5 μL of $PbBr_2$ solution (18 mg of $PbBr_2$ dissolved in 850 μL of OA and 850 μL of OLAM) was added to each vial. After 10 min, each sample was treated with 250 μL of toluene and 50 μL of TEOS (or 32.5 μL of TMOS). The completeness of the silica thickening was tested twice daily by withdrawing an aliquot of the sample and mixing it with OLAM-I under UV light. If the green-emissive sample turned orange-/red-emissive (substitution of Br^- with I^-),[50] then the shell overgrowth was deemed incomplete, and 1 μL of water was added to the reaction mixture to catalyze TEOS hydrolysis.[48] Once the halide exchange in the aliquot was suppressed (after 24–48 h for TEOS, 12–24 h for TMOS, depending on the batch), the $CsPbBr_3$@SiO_2@SiO_2 NCs were collected by precipitation with ethyl acetate (250 μL, followed by centrifugation at 4000 rpm for 5 min) and redispersion of the precipitate in 250 μL of toluene.

Optical Measurements. The UV–vis absorption spectra were recorded with a Cary 300 spectrophotometer. The PL spectra were recorded with a Varian Cary Eclipse with an excitation wavelength of 350 nm for all spectra. All measurements were performed in quartz cuvettes (10 mm optical path) filled with ~1 mL of sample dispersed in toluene solvent. The absolute PLQY measurements were carried out with an Edinburgh FLS920 spectrofluorimeter equipped with a calibrated integrating sphere and an excitation wavelength of 400 nm (Xe lamp), as detailed elsewhere.[48]

X-ray Diffraction (XRD). XRD measurements were performed with a PANalytical Empyrean X-ray diffractometer equipped with a 1.8 kW Cu Kα ceramic X-ray tube and a PIXcel3D 2 × 2 area detector, working at 45 kV and 40 mA under ambient conditions with the parallel beam geometry and symmetric reflection mode. The samples were prepared by drop-casting the NC solution onto a zero-diffraction silicon substrate and analyzed after the solvent evaporation.

Transmission Electron Microscopy (TEM). Bright-field TEM (BF-TEM) images were acquired with a JEOL JEM-1011 (W filament), operated at 100 kV accelerating voltage. The average NC dimensions were estimated using the ilastik image analysis tool.[51] The samples were prepared by drop-casting the solution onto carbon-coated Cu grids (200 mesh). High-resolution TEM (HR-TEM), energy-filtered TEM (EF-TEM), high-angle annular dark-field-scanning TEM (HAADF-STEM) imaging, and energy-dispersive X-ray spectroscopy (EDS) analyses were carried out on a JEOL JEM-2200FS TEM (Schottky emitter), operated at 200 kV accelerating voltage, equipped with a CEOS C_S-corrector for the objective lens, an in-column image filter (Ω-type), and a Bruker XFlash 5060 silicon-drift detector for EDS. The sample suspension (in toluene) was drop-cast onto an ultrathin carbon-coated Cu grid (150 mesh). Prior to elemental mapping (STEM-EDS and EF-TEM), the TEM grids underwent a thermal treatment (7 h at 80 °C in high vacuum) aimed at minimizing carbon contamination upon prolonged electron-beam irradiation. The STEM-EDS elemental maps presented here are obtained by integrating the K peak of oxygen, the Kα peaks of Si and Br, and the Lα peaks of Cs and Pb.

Nuclear Magnetic Resonance (NMR). Samples for NMR were prepared in a nitrogen-filled glovebox. A MANH stock solution (74 mg; 0.75 mmol) in 1.8 mL of deuterated toluene was prepared and kept under stirring for 1 h. Then, 0.6 mL of MANH stock solution was transferred into 5 mm disposable NMR tubes, and various

https://doi.org/10.1021/acs.chemmater.1c03749
Chem. Mater. 2022, 34, 405–413

amounts of degassed OLAM (33 μL or 0.1 mmol; 55 μL or 0.17 mmol; 85 μL or 0.25 mmol) were added. All the spectra were acquired at a temperature of 300 K with a Bruker Avance 400 MHz spectrometer, equipped with a BBI probe and Z-gradients, operating at 400.13 MHz (^{1}H) and 100.62 MHz (^{13}C), respectively. The full details of the NMR experiments are described in the Supporting Information.

RESULTS AND DISCUSSION

The as-synthesized Cs_4PbBr_6 NCs appeared roughly spherical with a diameter of 11.7 ± 1.3 nm (Figure 1a), a rhombohedral crystal structure (Figure 1g), an absorption peak at 314 nm (Figure 1h), and no PL emission. Upon addition of MANH and alkoxysilane, Cs_4PbBr_6 NCs reacted to produce $CsPbBr_3$@SiO_2 NCs in a one-step procedure (Scheme 1, steps 1 and 2 combined). Figure 1b shows a BF-TEM image of one of the best samples that display a clear core−shell morphology of the NC product (additional images of other syntheses are shown in Figure S1). The use of TEOS brought the best core−shell NC morphology, while TMOS gave more reproducible results. HR-TEM imaging and elemental analysis with STEM-EDS on the best sample revealed NCs composed of ∼10 nm single-crystal $CsPbBr_3$ cores coated by ∼5−7 nm-thick amorphous SiO_2 shells (Figure 1c−e, Figure S2). The core−shell sample demonstrated green emission, with a PL peak centered at 507 nm and a full width at half maximum of ∼20 nm (Figure 1h) and a low PLQY (∼1−4%). Its optical absorption spectrum featured one peak at lower (497 nm) and one at higher (314 nm) energies, ascribable to the band edge absorption of $CsPbBr_3$ NCs and Cs_4PbBr_6 NCs, respectively (Figure 1h). The coexistence of both Cs_4PbBr_6 and $CsPbBr_3$ phases was also confirmed by XRD (Figure 1f), suggesting a partial Cs_4PbBr_6 → $CsPbBr_3$ conversion. The absence of other phases in the XRD pattern corroborates the electron microscopy observations of a thin, amorphous silica shell.

To gain insight into the one-step synthesis of core−shell NCs, we analyzed aliquots of the reaction mixture taken at different reaction times. It was found that the formation of $CsPbBr_3$ from Cs_4PbBr_6 NCs and the silica growth occurred at different times. Specifically, approximately 20 s after the MANH addition, the clear and colorless dispersion of Cs_4PbBr_6 NCs turned yellow, indicating the formation of $CsPbBr_3$ NCs. Uncoated $CsPbBr_3$ NCs were observed via BF-TEM after ∼2 min of reaction, while the presence of SiO_2 became distinguishable only after ∼4 min (Figure S3). To further elucidate the reaction mechanism and disentangle the steps of Cs_4PbBr_6 → $CsPbBr_3$ conversion and SiO_2 growth, we performed a two-step synthesis of core−shell NCs. The two-step synthesis consists of the consecutive addition of MANH (Scheme 1, step 1) followed by TEOS (Scheme 1, step 2) after 15 min.

In the first step, the reaction between Cs_4PbBr_6 NCs (Figure 2a,f,g) and MANH stock solution yielded orthorhombic $CsPbBr_3$ NCs (with a residue of Cs_4PbBr_6) displaying an average lateral size of 7.9 ± 1.4 nm (Figure 2b,e), a PL emission peak with a maximum at 501 nm (Figure 2g), and a PLQY of ∼15%. In analogy with earlier work from our group,[45] the Cs_4PbBr_6 → $CsPbBr_3$ conversion was initiated by the condensation reaction of MANH (added in excess) with both the free OLAM and the OLAM bound to the surface of the Cs_4PbBr_6 NCs, to form maleamic acid (pK_a ∼ 3.5−4.0).[54,55] The reaction of OLAM with MANH and the formation of maleamic acid were confirmed by the ^{1}H and ^{13}C NMR analysis (Figure S4). We ascribe the modest PLQY of the $CsPbBr_3$ NCs to the defective surface or imperfect surface passivation with maleamic acid.

In the second step, we added TEOS to the crude solution of freshly formed $CsPbBr_3$ NCs after the Cs_4PbBr_6/MANH reaction. In this case, we observed the formation of core−shell structures with a silica coating thickness of about 10 nm, hence comparable with the one-step procedure (Figure 2c) that retained the orthorhombic $CsPbBr_3$ phase with residual Cs_4PbBr_6 (Figure 2d) and demonstrated a PL spectrum centered at 513 nm (Figure 2g). Considering the MANH-OLAM chemistry, it is reasonable to assume that the maleamic acid provided an acidic environment that catalyzed TEOS hydrolysis and a shell formation as a result. To test this assumption, we conducted two control experiments. In the first control experiment, we observed that if the $CsPbBr_3$ NCs were isolated from the reaction mixture after the Cs_4PbBr_6/MANH transformation, then no silica shell was formed around them upon addition of TEOS. This indicates that the acidic environment and reaction byproducts are required for silica shell formation. In the second control experiment, we used cesium oleate/oleylammonium-capped $CsPbBr_3$ NCs prepared via the hot-injection method[56] and observed no silica shell growth upon addition of TEOS (Figure S5). This observation indicates that $CsPbBr_3$ NCs derived from the reaction of Cs_4PbBr_6 NCs with MANH have a suitable surface reactivity to promote and withstand the growth of a silica shell.

The Cs_4PbBr_6/MANH reaction is not the only requirement for silica shell growth. Here, we note that when the one-step procedure was repeated under strictly moisture-free conditions using anhydrous reagents inside a nitrogen-filled glovebox, no silica was observed (Figure S6). We surmise that the adventitious water coming from air and present in non-anhydrous solvents is necessary for the hydrolysis of alkoxysilanes. This finding is consistent with prior reports of TEOS hydrolysis catalyzed by water traces in toluene.[57]

The $CsPbBr_3$@SiO_2 NCs synthesized in one- or two-step procedures had two shortcomings: low PLQY and a loss of PL intensity within minutes after immersion in ethanol (Figure 3e). The low PLQY of core−shell NCs is attributed to the surface traps, in analogy with PL quenching observed in SiO_2-capped CdSe nanoplatelets.[58,59] The poor stability of core−shell NCs against ethanol is attributed to the porosity of the SiO_2 shell or partial encapsulation of $CsPbBr_3$ cores.

To mitigate the first issue of low PL of $CsPbBr_3$@SiO_2 NCs, the samples were separately treated with a $PbBr_2$/OA/OLAM solution in toluene (Figure S7a) or Cs-oleate (Figure S7b) (the precursor used for the hot-injection synthesis of $CsPbBr_3$ NCs).[60−62] Both treatments increased the PL of the sample. The highest PLQY (8%) was measured after the addition of $PbBr_2$. Another sample treated with $PbBr_2$ experienced a negligible PL intensity drop over ∼19 days (Figure S7a). We attributed the relative enhancement in PL and PLQY to the surface passivation (rather than transformation of any residual Cs_4PbBr_6 material to extra $CsPbBr_3$ NCs) since the absorbance of $CsPbBr_3$ NCs did not show any appreciable increase after the treatment with the $PbBr_2$ solution (Figure S7c). The fact that these treatments altered the photophysics of the $CsPbBr_3$ cores supported the hypothesis that the SiO_2 shell displays porosity or defectiveness.

To tackle the second issue and make a thicker SiO_2 shell, we performed an extra silica-growing step using TEOS and obtained what we call $CsPbBr_3$@SiO_2@SiO_2 NCs (Figure 3,

https://doi.org/10.1021/acs.chemmater.1c03749
Chem. Mater. 2022, 34, 405−413

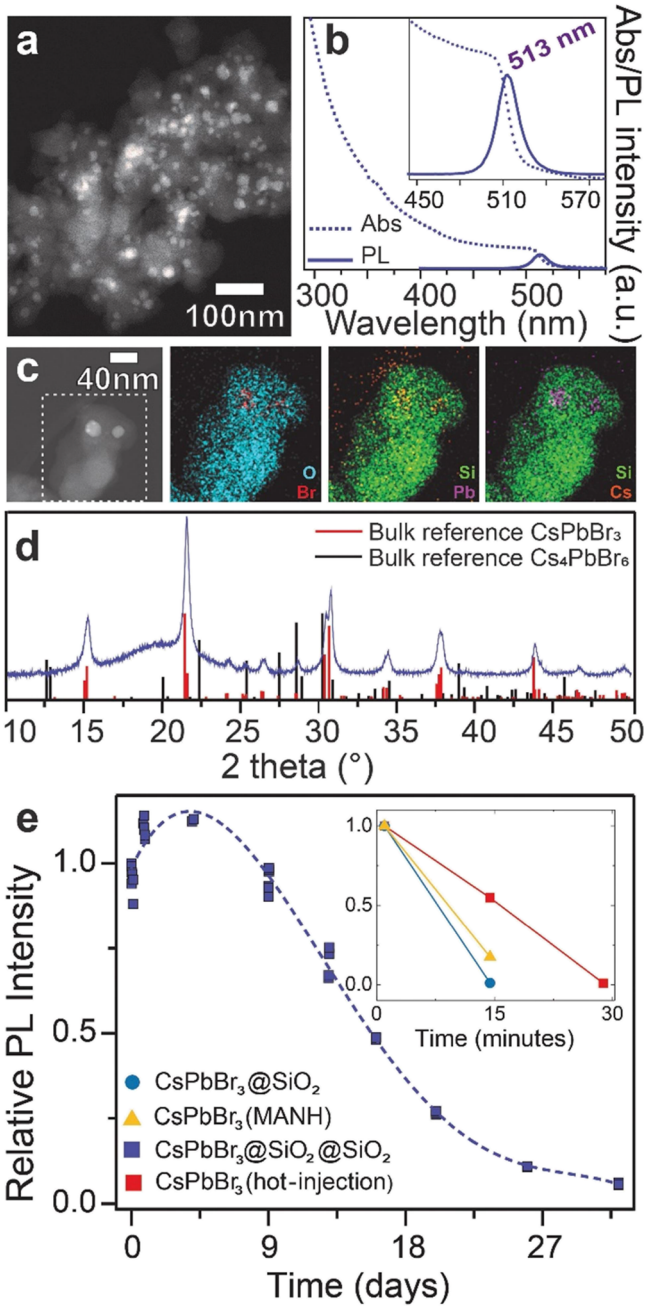

Figure 3. Characterization of $CsPbBr_3@SiO_2@SiO_2$ NCs and stability tests in ethanol. (a) Overview HAADF-STEM image; (b) optical absorption and PL spectra; (c) high-magnification HAADF-STEM image and corresponding EDS elemental maps; (d) XRD pattern of the $CsPbBr_3@SiO_2@SiO_2$ NC sample and the reference powder diffraction data for rhombohedral Cs_4PbBr_6 (black bars, ICSD code 162158) and orthorhombic $CsPbBr_3$ (red bars, COD code 4510745); (e) comparative quenching of PL intensity over time for four NC samples immersed in ethanol: $CsPbBr_3@SiO_2@SiO_2$, $CsPbBr_3@SiO_2$, $CsPbBr_3$ (MANH), and $CsPbBr_3$ (hot-injection).

for additional HAADF-STEM images, see Figure S8). The resulting particles had a thicker silica shell (estimated ~20 nm or more) around the perovskite core as compared to the initial $CsPbBr_3@SiO_2$ NCs. Atomic-number contrast HAADF-STEM imaging and EDS mapping identify the bright cores as the $CsPbBr_3$ NCs and the darker shell as the silica shell embedding them (Figure 3c). The second coating carried an additional benefit of removing the residual Cs_4PbBr_6, as evidenced by the disappearance of the 314 nm absorption peak (Figure 3b) and disappearance of Cs_4PbBr_6 reflections in XRD (Figure 3d). The PL peak position of the double-shelled sample underwent a redshift from 507 to 513 nm (Figure 3b), suggesting a coarsening of the $CsPbBr_3$ cores either due to ripening or further growth of $CsPbBr_3$ NCs from the consumed Cs_4PbBr_6. To access whether a thicker silica shell impacted the stability of $CsPbBr_3@SiO_2@SiO_2$ as compared to $CsPbBr_3$ and $CsPbBr_3@SiO_2$ NCs, we performed three stability tests: exposure to ethanol, photostability under 470 nm irradiation, and anion exchange with OLAM-I.

The $CsPbBr_3@SiO_2@SiO_2$ NCs exhibited increased stability in ethanol by retaining 95% of their initial PL intensity after 9 days of immersion in ethanol (dropping to 11% after the total of 26 days of continuous immersion, Figure 3e and Figure S9, see SI for details). For comparison, the PL of bare $CsPbBr_3$ NCs (either synthesized via Cs_4PbBr_6/MANH or hot-injection routes) and the PL of single-shelled $CsPbBr_3@SiO_2$ NCs were quenched after several minutes of ethanol exposure (Figure 3e) because of the accessible perovskite surface due to organic ligands and a defectiveness of the thin silica shell, respectively. Despite the PL retention in ethanol, the stability of the $CsPbBr_3@SiO_2@SiO_2$ NCs was poor in water: the PL intensity dropped to 40% of its initial value already after ~30 min of exposure to a toluene−water mixture (Figure S10, see SI for details).

In contrast to the ethanol exposure test, both $CsPbBr_3@SiO_2$ and $CsPbBr_3@SiO_2@SiO_2$ NC samples showed enhanced stability against 470 nm irradiation (Figures S11 and S12, LED source, I_{exc} = 100 mW·cm^{-2}, see SI for details). After 1 h of irradiation, the samples covered with silica showed ~10% ($CsPbBr_3@SiO_2@SiO_2$ NCs) and ~20% ($CsPbBr_3@SiO_2$ NCs) drop in the relative PL intensity. On the other hand, the uncoated samples demonstrated much faster photodegradation, exhibiting ~75% drop in relative PL intensity already after 10 min ($CsPbBr_3$ hot-injection) and 30 min ($CsPbBr_3$ MANH), respectively. Our results indicate that the photostability of the $CsPbBr_3$ NCs increases upon SiO_2 shelling.

Finally, the stability toward anion exchange was tested (Figure S13). $CsPbBr_3@SiO_2@SiO_2$ NCs (Figure S13a,c,e) and $CsPbBr_3$ NCs (Figure S13b,d,e) (hot-injection, control sample) were exposed to OLAM-I. The control sample changed its PL color from green to red within seconds after OLAM-I was added. After OLAM-I addition, the green PL of the $CsPbBr_3@SiO_2@SiO_2$ NCs first increased in intensity within the first ~5 min and gradually decreased afterward. At the same time, a PL peak at ~660 nm appeared after ~1 h and grew in intensity further shifting to ~675 nm on the subsequent day. These observations indicate that a thicker silica shell is insufficient to prevent anion exchange reactions. In the HAADF-STEM images of the starting $CsPbBr_3@SiO_2@SiO_2$ NCs, it is possible to see the occurrence of large pores (Figure S14) extending from the surface to the core, which, together with smaller and less visible pores, might explain why halide ions were able to reach the perovskite core.

CONCLUSIONS

In this work, we used the anhydride-mediated chemical transformation of Cs_4PbBr_6 into $CsPbBr_3$ NCs for the preparation of $CsPbBr_3@SiO_2$ core−shell NCs in the presence of alkoxysilanes. A combination of anhydride-amine con-

https://doi.org/10.1021/acs.chemmater.1c03749
Chem. Mater. 2022, 34, 405−413

densation that drives Cs_4PbBr_6 → $CsPbBr_3$ conversion and hydrolysis of alkoxysilanes could be seen as an alternative approach to colloidal atomic layer deposition developed to deposit alumina onto perovskite NCs.[63−65] The synthetic strategy presented here allows for the preparation of core−shell NCs and demonstrates the potential of transformative chemistry of metal halides for the fabrication of LHP-based nanoheterostructures. It would be interesting to extend this approach to NCs of other metal halides, e.g., Cs_4PbI_6 and Cs_4PbCl_6, as well as to other metal oxides that can be grown by wet chemistry approaches, e.g., TiO_2, ZrO_2, Al_2O_3, and SnO_2.

Aside from the proof-of-principle value of the presented results, the method and the resulting core−shell NCs have several shortcomings. The perovskite $CsPbBr_3$ NCs obtained from Cs_4PbBr_6 with MANH are poor emitters, and their PLQY is further lowered upon the coating with SiO_2. If one could find an effective treatment to boost the PLQY before the second silica coating step, the resulting materials would become attractive for applications relying on bright and stable emitters. The growth of the SiO_2 shell requires the presence of adventitious water, which makes it challenging to reproducibly prepare $CsPbBr_3$ cores uniformly coated with silica. In this respect, carrying out reactions under controlled humidity or with alternative alkoxysilane chemistries could result in reliable synthetic protocols compatible with large-scale production.

■ ASSOCIATED CONTENT

Supporting Information

The Supporting Information is available free of charge at https://pubs.acs.org/doi/10.1021/acs.chemmater.1c03749.

Additional experimental details of NMR characterization, ethanol and water stability tests, photostability tests; additional BF-TEM, EF-TEM, and HAADF-STEM images of the studied samples; ^1H and ^1H-^{13}C NMR spectra; summary of control experiments; PL spectra for chemically treated samples; PL spectra from photostability tests; and results of anion exchange tests (PDF)

■ AUTHOR INFORMATION

Corresponding Authors

Diego Colombara − *Nanochemistry Department, Italian Institute of Technology, Genova 16163, Italy; Department of Chemistry and Industrial Chemistry, University of Genova, Genova 16146, Italy;* orcid.org/0000-0002-8306-0994; Email: diego.colombara@bath.edu

Dmitry Baranov − *Nanochemistry Department, Italian Institute of Technology, Genova 16163, Italy;* orcid.org/0000-0001-6439-8132; Email: dmitry.baranov@iit.it

Authors

Christian Rossi − *Nanochemistry Department, Italian Institute of Technology, Genova 16163, Italy; Department of Chemistry and Industrial Chemistry, University of Genova, Genova 16146, Italy*

Riccardo Scarfiello − *CNR NANOTEC, Institute of Nanotechnology, Lecce 73100, Italy*

Rosaria Brescia − *Electron Microscopy Facility, Istituto Italiano di Tecnologia, Genova 16163, Italy;* orcid.org/0000-0003-0607-0627

Luca Goldoni − *Analytical Chemistry Lab, Istituto Italiano di Tecnologia, Genova 16163, Italy*

Gianvito Caputo − *Nanochemistry Department, Italian Institute of Technology, Genova 16163, Italy;* orcid.org/0000-0002-8973-3109

Luigi Carbone − *CNR NANOTEC, Institute of Nanotechnology, Lecce 73100, Italy*

Luca De Trizio − *Nanochemistry Department, Italian Institute of Technology, Genova 16163, Italy;* orcid.org/0000-0002-1514-6358

Liberato Manna − *Nanochemistry Department, Italian Institute of Technology, Genova 16163, Italy;* orcid.org/0000-0003-4386-7985

Complete contact information is available at: https://pubs.acs.org/10.1021/acs.chemmater.1c03749

Author Contributions

The manuscript was written through the contributions of all authors. All authors have given approval to the final version of the manuscript.

Notes

The authors declare no competing financial interest.

■ ACKNOWLEDGMENTS

The authors thank Nanochemistry and Analytical Chemistry Laboratories at IIT, Materials Characterization and Electron Microscopy facilities at IIT for training, technical support, and access to the instrumentation used to carry out the described experiments.

■ ABBREVIATIONS

COD, crystallography open database; EDS, energy-dispersive X-ray spectroscopy; ICSD, inorganic crystal structure database; LED, light-emitting diode; LHP, lead halide perovskite; MANH, maleic anhydride; MOF, metal−organic framework; NC, nanocrystal; NMR, nuclear magnetic resonance; OA, oleic acid; ODE, 1-octadecene; OLAM, oleylamine; OLAM-I, OLAM-iodide; PL, photoluminescence; PLQY, PL quantum yield; TEM, transmission electron microscopy; BF-TEM, bright-field TEM; EF-TEM, energy-filtered TEM; HR-TEM, high-resolution TEM; STEM, scanning TEM; HAADF-STEM, high-angle annular dark-field STEM; TEOS, tetraethyl orthosilicate; TMOS, tetramethyl orthosilicate; XRD, X-ray diffraction

■ REFERENCES

(1) Gao, L.; Yan, Q. Recent Advances in Lead Halide Perovskites for Radiation Detectors. *Sol. RRL* **2020**, *4*, No. 1900210.

(2) Zhao, H.; Zhou, Y.; Benetti, D.; Ma, D.; Rosei, F. Perovskite Quantum Dots Integrated in Large-Area Luminescent Solar Concentrators. *Nano Energy* **2017**, *37*, 214−223.

(3) Gandini, M.; Villa, I.; Beretta, M.; Gotti, C.; Imran, M.; Carulli, F.; Fantuzzi, E.; Sassi, M.; Zaffalon, M.; Brofferio, C.; Manna, L.; Beverina, L.; Vedda, A.; Fasoli, M.; Gironi, L.; Brovelli, S. Efficient, Fast and Reabsorption-Free Perovskite Nanocrystal-Based Sensitized Plastic Scintillators. *Nat. Nanotechnol.* **2020**, *15*, 462−468.

(4) Hao, M.; Bai, Y.; Zeiske, S.; Ren, L.; Liu, J.; Yuan, Y.; Zarrabi, N.; Cheng, N.; Ghasemi, M.; Chen, P.; Lyu, M.; He, D.; Yun, J. H.; Du, Y.; Wang, Y.; Ding, S.; Armin, A.; Meredith, P.; Liu, G.; Cheng, H. M.; Wang, L. Ligand-Assisted Cation-Exchange Engineering for High-Efficiency Colloidal $Cs_{1-x}FA_xPbI_3$ Quantum Dot Solar Cells with Reduced Phase Segregation. *Nat. Energy* **2020**, *5*, 79−88.

(5) Cheng, L. P.; Huang, J. S.; Shen, Y.; Li, G. P.; Liu, X. K.; Li, W.; Wang, Y. H.; Li, Y. Q.; Jiang, Y.; Gao, F.; Lee, C. S.; Tang, J. X. Efficient $CsPbBr_3$ Perovskite Light-Emitting Diodes Enabled by

Synergetic Morphology Control. *Adv. Opt. Mater.* **2019**, *7*, No. 1801534.
(6) Xu, L.; Yuan, S.; Zeng, H.; Song, J. A Comprehensive Review of Doping in Perovskite Nanocrystals/Quantum Dots: Evolution of Structure, Electronics, Optics, and Light-Emitting Diodes. *Mater. Today Nano* **2019**, *6*, No. 100036.
(7) Wei, Y.; Cheng, Z.; Lin, J. An Overview on Enhancing the Stability of Lead Halide Perovskite Quantum Dots and Their Applications in Phosphor-Converted LEDs. *Chem. Soc. Rev.* **2019**, *48*, 310−350.
(8) Deschler, F.; Price, M.; Pathak, S.; Klintberg, L. E.; Jarausch, D. D.; Higler, R.; Hüttner, S.; Leijtens, T.; Stranks, S. D.; Snaith, H. J.; Atatüre, M.; Phillips, R. T.; Friend, R. H. High Photoluminescence Efficiency and Optically Pumped Lasing in Solution-Processed Mixed Halide Perovskite Semiconductors. *J. Phys. Chem. Lett.* **2014**, *5*, 1421−1426.
(9) Schmidt, L. C.; Pertegás, A.; González-Carrero, S.; Malinkiewicz, O.; Agouram, S.; Mínguez Espallargas, G.; Bolink, H. J.; Galian, R. E.; Pérez-Prieto, J. Nontemplate Synthesis of $CH_3NH_3PbBr_3$ Perovskite Nanoparticles. *J. Am. Chem. Soc.* **2014**, *136*, 850−853.
(10) Gonzalez-Carrero, S.; Francés-Soriano, L.; González-Béjar, M.; Agouram, S.; Galian, R. E.; Pérez-Prieto, J. The Luminescence of $CH_3NH_3PbBr_3$ Perovskite Nanoparticles Crests the Summit and Their Photostability under Wet Conditions Is Enhanced. *Small* **2016**, *12*, 5245−5250.
(11) Protesescu, L.; Yakunin, S.; Bodnarchuk, M. I.; Krieg, F.; Caputo, R.; Hendon, C. H.; Yang, R. X.; Walsh, A.; Kovalenko, M. V. Nanocrystals of Cesium Lead Halide Perovskites ($CsPbX_3$, X = Cl, Br, and I): Novel Optoelectronic Materials Showing Bright Emission with Wide Color Gamut. *Nano Lett.* **2015**, *15*, 3692−3696.
(12) Yang, W.; Gao, F.; Qiu, Y.; Liu, W.; Xu, H.; Yang, L.; Liu, Y. $CsPbBr_3$-Quantum-Dots/Polystyrene@Silica Hybrid Microsphere Structures with Significantly Improved Stability for White LEDs. *Adv. Opt. Mater.* **2019**, *7*, No. 1900546.
(13) An, M. N.; Park, S.; Brescia, R.; Lutfullin, M.; Sinatra, L.; Bakr, O. M.; De Trizio, L.; Manna, L. Low-Temperature Molten Salts Synthesis: $CsPbBr_3$ Nanocrystals with High Photoluminescence Emission Buried in Mesoporous SiO_2. *ACS Energy Lett.* **2021**, *6*, 900−907.
(14) Park, S.; An, M. N.; Almeida, G.; Palazon, F.; Spirito, D.; Krahne, R.; Dang, Z.; De Trizio, L.; Manna, L. $CsPbX_3/SiO_x$ (X = Cl, Br, I) Monoliths Prepared via a Novel Sol-Gel Route Starting from Cs_4PbX_6 Nanocrystals. *Nanoscale* **2019**, *11*, 18739−18745.
(15) Li, Z. J.; Hofman, E.; Li, J.; Davis, A. H.; Tung, C. H.; Wu, L. Z.; Zheng, W. Photoelectrochemically Active and Environmentally Stable $CsPbBr_3/TiO_2$ Core/Shell Nanocrystals. *Adv. Funct. Mater.* **2018**, *28*, No. 1704288.
(16) Pan, A.; Wu, Y.; Yan, K.; Yu, Y.; Jurow, M. J.; Ren, B.; Zhang, C.; Ding, S.; He, L.; Liu, Y. Stable Luminous Nanocomposites of Confined Mn^{2+}-Doped Lead Halide Perovskite Nanocrystals in Mesoporous Silica Nanospheres as Orange Fluorophores. *Inorg. Chem.* **2019**, *58*, 3950−3958.
(17) Qian, C. X.; Deng, Z. Y.; Yang, K.; Feng, J.; Wang, M. Z.; Yang, Z.; Liu, S.; Feng, H. J. Interface Engineering of $CsPbBr_3/TiO_2$ Heterostructure with Enhanced Optoelectronic Properties for All-Inorganic Perovskite Solar Cells. *Appl. Phys. Lett.* **2018**, *112*, No. 093901.
(18) Chen, P.; Liu, Y.; Zhang, Z.; Sun, Y.; Hou, J.; Zhao, G.; Zou, J.; Fang, Y.; Xu, J.; Dai, N. In Situ Growth of Ultrasmall Cesium Lead Bromine Quantum Dots in a Mesoporous Silica Matrix and Their Application in Flexible Light-Emitting Diodes. *Nanoscale* **2019**, *11*, 16499−16507.
(19) Dirin, D. N.; Protesescu, L.; Trummer, D.; Kochetygov, I. V.; Yakunin, S.; Krumeich, F.; Stadie, N. P.; Kovalenko, M. V. Harnessing Defect-Tolerance at the Nanoscale: Highly Luminescent Lead Halide Perovskite Nanocrystals in Mesoporous Silica Matrixes. *Nano Lett.* **2016**, *16*, 5866−5874.
(20) Malgras, V.; Henzie, J.; Takei, T.; Yamauchi, Y. Stable Blue Luminescent $CsPbBr_3$ Perovskite Nanocrystals Confined in Mesoporous Thin Films. *Angew. Chem., Int. Ed.* **2018**, *57*, 8881−8885.
(21) Wang, H. C.; Lin, S. Y.; Tang, A. C.; Singh, B. P.; Tong, H. C.; Chen, C. Y.; Lee, Y. C.; Tsai, T. L.; Liu, R. S. Mesoporous Silica Particles Integrated with All-Inorganic $CsPbBr_3$ Perovskite Quantum-Dot Nanocomposites (MP-PQDs) with High Stability and Wide Color Gamut Used for Backlight Display. *Angew. Chem., Int. Ed.* **2016**, *55*, 7924−7929.
(22) Zhang, Q.; Wang, B.; Zheng, W.; Kong, L.; Wan, Q.; Zhang, C.; Li, Z.; Cao, X.; Liu, M.; Li, L. Ceramic-like Stable $CsPbBr_3$ Nanocrystals Encapsulated in Silica Derived from Molecular Sieve Templates. *Nat. Commun.* **2020**, *11*, 31.
(23) Zhang, Q.; Sun, X.; Zheng, W.; Wan, Q.; Liu, M.; Liao, X.; Hagio, T.; Ichino, R.; Kong, L.; Wang, H.; Li, L. Band Gap Engineering toward Wavelength Tunable $CsPbBr_3$ Nanocrystals for Achieving Rec. 2020 Displays. *Chem. Mater.* **2021**, *33*, 3575−3584.
(24) Raja, S. N.; Bekenstein, Y.; Koc, M. A.; Fischer, S.; Zhang, D.; Lin, L.; Ritchie, R. O.; Yang, P.; Alivisatos, A. P. Encapsulation of Perovskite Nanocrystals into Macroscale Polymer Matrices: Enhanced Stability and Polarization. *ACS Appl. Mater. Interfaces* **2016**, *8*, 35523−35533.
(25) Li, X.; Xue, Z.; Luo, D.; Huang, C.; Liu, L.; Qiao, X.; Liu, C.; Song, Q.; Yan, C.; Li, Y.; Wang, T. A Stable Lead Halide Perovskite Nanocrystals Protected by PMMA. *Sci. China Mater.* **2018**, *61*, 363−370.
(26) Hou, S.; Guo, Y.; Tang, Y.; Quan, Q. Synthesis and Stabilization of Colloidal Perovskite Nanocrystals by Multidentate Polymer Micelles. *ACS Appl. Mater. Interfaces* **2017**, *9*, 18417−18422.
(27) Lin, C. C.; Jiang, D. H.; Kuo, C. C.; Cho, C. J.; Tsai, Y. H.; Satoh, T.; Su, C. Water-Resistant Efficient Stretchable Perovskite-Embedded Fiber Membranes for Light-Emitting Diodes. *ACS Appl. Mater. Interfaces* **2018**, *10*, 2210−2215.
(28) Shi, J.; Ge, W.; Gao, W.; Xu, M.; Zhu, J.; Li, Y. Enhanced Thermal Stability of Halide Perovskite $CsPbX_3$ Nanocrystals by a Facile TPU Encapsulation. *Adv. Opt. Mater.* **2020**, *8*, No. 1901516.
(29) Dirin, D. N.; Benin, B. M.; Yakunin, S.; Krumeich, F.; Raino, G.; Frison, R.; Kovalenko, M. V. Microcarrier-Assisted Inorganic Shelling of Lead Halide Perovskite Nanocrystals. *ACS Nano* **2019**, *13*, 11642−11652.
(30) Ren, J.; Li, T.; Zhou, X.; Dong, X.; Shorokhov, A. V.; Semenov, M. B.; Krevchik, V. D.; Wang, Y. Encapsulating All-Inorganic Perovskite Quantum Dots into Mesoporous Metal Organic Frameworks with Significantly Enhanced Stability for Optoelectronic Applications. *Chem. Eng. J.* **2019**, *358*, 30−39.
(31) Bera, S.; Pradhan, N. Perovskite Nanocrystal Heterostructures: Synthesis, Optical Properties, and Applications. *ACS Energy Lett.* **2020**, *5*, 2858−2872.
(32) Ren, J.; Zhou, X.; Wang, Y. Dual-Emitting $CsPbX_3$@ZJU-28 (X = Cl, Br, I) Composites with Enhanced Stability and Unique Optical Properties for Multifunctional Applications. *Chem. Eng. J.* **2020**, *391*, No. 123622.
(33) Wang, Y.; He, J.; Chen, H.; Chen, J.; Zhu, R.; Ma, P.; Towers, A.; Lin, Y.; Gesquiere, A. J.; Wu, S. T.; Dong, Y. Ultrastable, Highly Luminescent Organic−Inorganic Perovskite−Polymer Composite Films. *Adv. Mater.* **2016**, *28*, 10710−10717.
(34) Zhang, D.; Xu, Y.; Liu, Q.; Xia, Z. Encapsulation of $CH_3NH_3PbBr_3$ Perovskite Quantum Dots in MOF-5 Microcrystals as a Stable Platform for Temperature and Aqueous Heavy Metal Ion Detection. *Inorg. Chem.* **2018**, *57*, 4613−4619.
(35) Malgras, V.; Tominaka, S.; Ryan, J. W.; Henzie, J.; Takei, T.; Ohara, K.; Yamauchi, Y. Observation of Quantum Confinement in Monodisperse Methylammonium Lead Halide Perovskite Nanocrystals Embedded in Mesoporous Silica. *J. Am. Chem. Soc.* **2016**, *138*, 13874−13881.
(36) Cheng, J.; Yuan, S.; Zhu, L.; Chen, L.; Liu, C.; Tong, H.; Zeng, H. Room-Temperature In Situ Synthesis of a Highly Efficient $CsPbBr_3/SiO_2$ Sol Entirely in Ethanol Solvent by Constructing

Amine-Functionalized Silica Micelles. *Langmuir* **2020**, *36*, 6017−6024.
(37) Zhong, Q.; Cao, M.; Hu, H.; Yang, D.; Chen, M.; Li, P.; Wu, L.; Zhang, Q. One-Pot Synthesis of Highly Stable $CsPbBr_3$@SiO_2 Core-Shell Nanoparticles. *ACS Nano* **2018**, *12*, 8579−8587.
(38) Meng, C.; Yang, D.; Wu, Y.; Zhang, X.; Zeng, H.; Li, X. Synthesis of Single $CsPbBr_3$@SiO_2 Core-Shell Particles: Via Surface Activation. *J. Mater. Chem. C* **2020**, *8*, 17403−17409.
(39) Zhao, H.; Wei, L.; Zeng, P.; Liu, M. Formation of Highly Uniform Thinly-Wrapped $CsPbX_3$@silicone Nanocrystals via Self-Hydrolysis: Suppressed Anion Exchange and Superior Stability in Polar Solvents. *J. Mater. Chem. C* **2019**, *7*, 9813−9819.
(40) Song, W.; Wang, Y.; Wang, B.; Yao, Y.; Wang, W.; Wu, J.; Shen, Q.; Luo, W.; Zou, Z. Super Stable $CsPbBr_3$@SiO_2 Tumor Imaging Reagent by Stress-Response Encapsulation. *Nano Res.* **2020**, *13*, 795−801.
(41) Gao, F.; Yang, W.; Liu, X.; Li, Y.; Liu, W.; Xu, H.; Liu, Y. Highly Stable and Luminescent Silica-Coated Perovskite Quantum Dots at Nanoscale-Particle Level via Nonpolar Solvent Synthesis. *Chem. Eng. J.* **2021**, *407*, No. 128001.
(42) Kumar, P.; Patel, M.; Park, C.; Han, H.; Jeong, B.; Kang, H.; Patel, R.; Koh, W.-G.; Park, C. Highly Luminescent Biocompatible $CsPbBr_3$@SiO_2 Core−Shell Nanoprobes for Bioimaging and Drug Delivery. *J. Mater. Chem. B* **2020**, *8*, 10337−10345.
(43) Nandiyanto, A. B. D.; Kim, S. G.; Iskandar, F.; Okuyama, K. Synthesis of Spherical Mesoporous Silica Nanoparticles with Nanometer-Size Controllable Pores and Outer Diameters. *Microporous Mesoporous Mater.* **2009**, *120*, 447−453.
(44) Stöber, W.; Fink, A.; Bohn, E. Controlled Growth of Monodisperse Silica Spheres in the Micron Size Range. *J. Colloid Interface Sci.* **1968**, *26*, 62−69.
(45) Baranov, D.; Caputo, G.; Goldoni, L.; Dang, Z.; Scarfiello, R.; De Trizio, L.; Portone, A.; Fabbri, F.; Camposeo, A.; Pisignano, D.; Manna, L. Transforming Colloidal Cs_4PbBr_6 Nanocrystals with Poly(Maleic Anhydride- Alt −1-Octadecene) into Stable $CsPbBr_3$ Perovskite Emitters through Intermediate Heterostructures. *Chem. Sci.* **2020**, *11*, 3986−3995.
(46) Jin, Z.; Du, L.; Zhang, C.; Sugiyama, Y.; Wang, W.; Palui, G.; Wang, S.; Mattoussi, H. Modification of Poly(Maleic Anhydride)-Based Polymers with H_2N−R Nucleophiles: Addition or Substitution Reaction? *Bioconjugate Chem.* **2019**, *30*, 871−880.
(47) Wang, S.; Du, L.; Jin, Z.; Xin, Y.; Mattoussi, H. Enhanced Stabilization and Easy Phase Transfer of $CsPbBr_3$ Perovskite Quantum Dots Promoted by High-Affinity Polyzwitterionic Ligands. *J. Am. Chem. Soc.* **2020**, *142*, 12669−12680.
(48) Akkerman, Q. A.; Martínez-Sarti, L.; Goldoni, L.; Imran, M.; Baranov, D.; Bolink, H. J.; Palazon, F.; Manna, L. Molecular Iodine for a General Synthesis of Binary and Ternary Inorganic and Hybrid Organic-Inorganic Iodide Nanocrystals. *Chem. Mater.* **2018**, *30*, 6915−6921.
(49) Akkerman, Q. A.; Park, S.; Radicchi, E.; Nunzi, F.; Mosconi, E.; De Angelis, F.; Brescia, R.; Rastogi, P.; Prato, M.; Manna, L. Nearly Monodisperse Insulator Cs_4PbX_6 (X = Cl, Br, I) Nanocrystals, Their Mixed Halide Compositions, and Their Transformation into $CsPbX_3$ Nanocrystals. *Nano Lett.* **2017**, *17*, 1924−1930.
(50) Akkerman, Q. A.; D'Innocenzo, V.; Accornero, S.; Scarpellini, A.; Petrozza, A.; Prato, M.; Manna, L. Tuning the Optical Properties of Cesium Lead Halide Perovskite Nanocrystals by Anion Exchange Reactions. *J. Am. Chem. Soc.* **2015**, *137*, 10276−10281.
(51) Berg, S.; Kutra, D.; Kroeger, T.; Straehle, C. N.; Kausler, B. X.; Haubold, C.; Schiegg, M.; Ales, J.; Beier, T.; Rudy, M.; Eren, K.; Cervantes, J. I.; Xu, B.; Beuttenmueller, F.; Wolny, A.; Zhang, C.; Koethe, U.; Hamprecht, F. A.; Kreshuk, A. Ilastik: Interactive Machine Learning for (Bio)Image Analysis. *Nat. Methods* **2019**, *16*, 1226−1232.
(52) Akkerman, Q. A.; Motti, S. G.; Srimath Kandada, A. R.; Mosconi, E.; D'Innocenzo, V.; Bertoni, G.; Marras, S.; Kamino, B. A.; Miranda, L.; De Angelis, F.; Petrozza, A.; Prato, M.; Manna, L. Solution Synthesis Approach to Colloidal Cesium Lead Halide Perovskite Nanoplatelets with Monolayer-Level Thickness Control. *J. Am. Chem. Soc.* **2016**, *138*, 1010−1016.
(53) Brennan, M. C.; Kuno, M.; Rouvimov, S. Crystal Structure of Individual $CsPbBr_3$ Perovskite Nanocubes. *Inorg. Chem.* **2019**, *58*, 1555−1560.
(54) Ronald, K.; Jik, C.; Choy, W. W. Carboxylic Acid Participation in Amide Hydrolysis. Reactivity of Intermediates in the Internally Catalyzed Hydrolysis of N-Substituted 2,3-Dimethylmaleamic Acids. *J. Am. Chem. Soc.* **1979**, *101*, 6976−6980.
(55) Suh, J.; Kim, M. J.; Seong, N. J. Ionization and Intramolecular Reactions of N,N-Bis[(2-Pyridyl)Ethyl]- and N,N-Bis[(2-Pyridyl)-MethyI]Maleamic Acids. An Enzyme Model. *J. Org. Chem.* **1981**, *46*, 4354−4358.
(56) Baranov, D.; Toso, S.; Imran, M.; Manna, L. Investigation into the Photoluminescence Red Shift in Cesium Lead Bromide Nanocrystal Superlattices. *J. Phys. Chem. Lett.* **2019**, *10*, 655−660.
(57) Huang, S.; Li, Z.; Kong, L.; Zhu, N.; Shan, A.; Li, L. Enhancing the Stability of $CH_3NH_3PbBr_3$ Quantum Dots by Embedding in Silica Spheres Derived from Tetramethyl Orthosilicate in "Waterless" Toluene. *J. Am. Chem. Soc.* **2016**, *138*, 5749−5752.
(58) Hutter, E. M.; Pietra, F.; van Dijk - Moes, R. J. A.; Mitoraj, D.; Meeldijk, J. D.; de Mello Donegá, C.; Vanmaekelbergh, D. Method To Incorporate Anisotropic Semiconductor Nanocrystals of All Shapes in an Ultrathin and Uniform Silica Shell. *Chem. Mater.* **2014**, *26*, 1905−1911.
(59) Hutter, E. M.; Bladt, E.; Goris, B.; Pietra, F.; van der Bok, J. C.; Boneschanscher, M. P.; de Mello Donegá, C.; Bals, S.; Vanmaekelbergh, D. Conformal and Atomic Characterization of Ultrathin CdSe Platelets with a Helical Shape. *Nano Lett.* **2014**, *14*, 6257−6262.
(60) Bodnarchuk, M. I.; Boehme, S. C.; Ten Brinck, S.; Bernasconi, C.; Shynkarenko, Y.; Krieg, F.; Widmer, R.; Aeschlimann, B.; Günther, D.; Kovalenko, M. V.; Infante, I. Rationalizing and Controlling the Surface Structure and Electronic Passivation of Cesium Lead Halide Nanocrystals. *ACS Energy Lett.* **2019**, *4*, 63−74.
(61) Aristidou, N.; Eames, C.; Sanchez-Molina, I.; Bu, X.; Kosco, J.; Islam, M. S.; Haque, S. A. Fast Oxygen Diffusion and Iodide Defects Mediate Oxygen-Induced Degradation of Perovskite Solar Cells. *Nat. Commun.* **2017**, *8*, 15218.
(62) Bohn, B. J.; Tong, Y.; Gramlich, M.; Lai, M. L.; Döblinger, M.; Wang, K.; Hoye, R. L. Z.; Müller-Buschbaum, P.; Stranks, S. D.; Urban, A. S.; Polavarapu, L.; Feldmann, J. Boosting Tunable Blue Luminescence of Halide Perovskite Nanoplatelets through Post-synthetic Surface Trap Repair. *Nano Lett.* **2018**, *18*, 5231−5238.
(63) Loiudice, A.; Strach, M.; Saris, S.; Chernyshov, D.; Buonsanti, R. Universal Oxide Shell Growth Enables in Situ Structural Studies of Perovskite Nanocrystals during the Anion Exchange Reaction. *J. Am. Chem. Soc.* **2019**, *141*, 8254−8263.
(64) Loiudice, A.; Saris, S.; Buonsanti, R. Tunable Metal Oxide Shell as a Spacer to Study Energy Transfer in Semiconductor Nanocrystals. *J. Phys. Chem. Lett.* **2020**, *11*, 3430−3435.
(65) Loiudice, A.; Segura Lecina, O.; Buonsanti, R. Atomic Control in Multicomponent Nanomaterials: When Colloidal Chemistry Meets Atomic Layer Deposition. *ACS Mater. Lett.* **2020**, *2*, 1182−1202.